Steady-State Load Identification Method of Inductive Power Transfer System Based on Switching Capacitors

Yu-Gang Su, *Member, IEEE*, Hong-Yan Zhang, Zhi-Hui Wang, *Member, IEEE*, Aiguo Patrick Hu, *Senior Member, IEEE*, Long Chen, and Yue Sun, *Member, IEEE*

***Abstract*—An online steady-state load identification method is proposed to solve the problems related to frequency drift, system robustness deterioration, difficulties in controller design due to the uncertainties in load and mutual inductance variations of an inductive power transfer (IPT) system. Take a Series-Series-type IPT system as an example, an additional capacitor is added into the system to make the system work in two operating modes, and a mathematical model is established according to the two modes for the system identification. Simulation and experimental results have verified the proposed online load identification method. It has demonstrated that the method is accurate and reliable for identifying uncertain loads and magnetic coupling variations if other system parameters are known. The method can be used to improve the system performance with precise control.**

***Index Terms*—Inductive power transfer (IPT), load identification, resonance, reflected impedance.**

NOMENCLATURE

$E_{\rm DC}, u_p$	The voltage of dc link and output voltage of the inverter, respectively.
L_p, L_s	Resonant inductances of the primary and secondary circuits, respectively.
R_p, R_s	The inherent resistances of the primary and secondary windings, respectively.
C_p, C_s	The compensating capacitances of the primary and secondary circuits, respectively.
C_1, C_2	The compensating capacitances of the primary side.
M	Mutual inductance between the primary and secondary windings.
Z_L	Equivalent impedance.
R_L	Equivalent load.
Z_r	Reflected impedance of the secondary side to the primary side.
$\mathrm{Re}Z_r, \mathrm{Im}Z_r$	The real and imaginary parts of Z_r.
Z_p	Total impedance of the primary side.
I_p	The RMS of the primary resonant current.
$\omega_{\rm ref}$	The natural resonant frequency of the secondary side.
$\omega_{\rm ref1}$	The hard switching frequency after switching the compensation capacitor of the primary side.

Manuscript received September 30, 2014; revised January 4, 2015; accepted March 1, 2015. Date of publication March 11, 2015; date of current version July 10, 2015. This work was supported by the National Natural Science Foundation of China under Grants 51477020, 51207173, and 51377183. Recommended for publication by Associate Editor G. A. Covic.

Y.-G. Su, H.-Y. Zhang, Z.-H. Wang, and L. Chen are with the College of Automation, Chongqing University, Chongqing 400044, China (e-mail: su7558@qq.com; hyanzhang1991@163.com; wzhcqu@hotmail.com; cheney0118@qq.com).

A.-P. Hu is with the Department of Electrical and Computer Engineering, University of Auckland, Auckland 1142, New Zealand (e-mail: a.hu@auckland.ac.nz).

Y. Sun is with the State Key Laboratory of Power Transmission Equipment & System Security and New Technology, and the College of Automation, Chongqing University, Chongqing 400044, China (e-mail: syue06@cqu.edu.cn).

Digital Object Identifier 10.1109/TPEL.2015.2411755

I. INTRODUCTION

INDUCTIVE power transfer (IPT) technology is based on electromagnetic coupling to supply power to electrical equipment without direct electrical contacts [1]–[3]. Because of its safety, convenience, and flexible features, IPT has been widely used for electric vehicles charging and power supplies to household appliances, implantable biomedical devices, as well as some other special situations where direct electrical contacts are inconvenient or impossible [4]–[12]. In an IPT system, the operating frequency of the system is normally designed to be the same as the resonant frequency of the secondary power pick-up to maximize the power transfer. However, one feature of an IPT system is that its magnetic field coupling and load can affect the system operating frequency [13]. As a result, the system efficiency and power transfer capacity will decrease dramatically.

In practical operation of an IPT system, the load change reflects the change in the actual power requirement, so the output power of the system should be adjusted to ensure efficient and reliable power transfer. Different energy receiving devices may present different loads and mutual inductances, causing large variations in the reflected impedance to the primary power supply [14], [15]. Take the wireless power supply for electric vehicles as an example, different electric vehicles have different power requirements as well as load characteristics, and different heights and alignment of chassis can cause the air gap between the transmitting winding and the pick-up winding to change, resulting in different mutual inductance. Therefore, the load and the mutual inductance identification of an IPT system is necessary, although features like nonlinearity, high order, and high frequency operation of an IPT system make it a very challenging task [16].

A few research works on the load identification of IPT system have been reported [17]–[19]. Literature [17] proposed a dynamic load identification method based on energy storage,

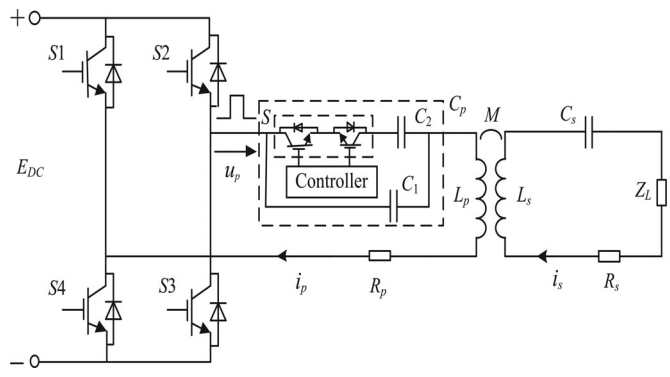

Fig. 1. SS-type IPT system with full-bridge inverter circuit based on capacitance switching.

power supply, and energy dissipation. Literature [18] achieves load identification by detecting the energy dissipation time of self-oscillation circuit in a wireless power supply to household appliances. Literature [19] proposes a method based on the current characteristics under ZVS condition of a current-fed IPT system. But the above load identification methods did not consider the mutual inductance variation, which is typical for practical operation of IPT systems with variable magnetic coupling between the primary and secondary coils.

This paper proposes a steady-state load identification method for unknown mutual inductance between the primary and secondary coils of an IPT system. The primary side works in resonance with variable compensation achieved by switching capacitors, and then the input voltage, current, and resonant frequency are detected. Assume other system parameters are known apart from the load and magnetic coupling variations, the impedance equations are established by combining the steady-state characteristics and the reflected impedance circuit model. Then the equivalent load impedance and mutual inductance are calculated. Finally, the simulation and experimental results have verified the feasibility and accuracy of the design method.

II. Proposed Method and Basic Operating Principle

A. Basic Circuit Topology Based on Switching Capacitor

An IPT system typically requires to be compensated in both primary side and secondary side in order to improve the power factor, lower the components stress, and increase the power transfer capability. Generally, there are two kinds of reactive power compensation methods which are voltage type and current type compensations [20], [21]. The primary and secondary windings can be either series or parallel compensated. This paper focuses on Series-Series (SS)-type voltage-fed IPT system and its diagram is shown in Fig. 1.

In the primary side, the full-bridge inverter network consists of four semiconductor switches (e.g., insulated-gate bipolar transistors (IGBTs) *S*1, *S*2, *S*3, and *S*4. The inverter network works in zero-current- switching (ZCS) soft switching mode, and the dc voltage $E_{\rm DC}$ is converted into a high-frequency alternating voltage u_p. The primary resonant network is made up of an inductor L_p and a compensating capacitor C_p. A high-frequency alternating current is generated across the resonant network, and a high-frequency magnetic field is created by primary winding.

In the secondary side, the power pick-up winding L_s receives power via the high-frequency magnetic field coupling. The series resonant network in secondary side consists of an inductor L_s and a compensating capacitor C_s. The pick-up side supplies power to the equivalent load Z_L via the resonant network.

B. Output Voltage of Inverter

The L_p and C_p is equivalent to a low-pass filter in energy transmitter winding. This filter shows a larger impedance of high-frequency harmonic voltage and reduces the high-frequency harmonic currents in the resonant network. In such a case, only the fundamental resonant frequency needs to be considered for power transfer. When the system works in soft-switching mode, the RMS output square wave voltage U_p of full-bridge inverter can be approximated as

$$U_p = \frac{4E_{\rm DC}}{\sqrt{2}\pi} = 0.9E_{\rm DC}. \tag{1}$$

C. Equivalent Load

For simplify, the load of IPT is often modeled as a pure resistance in previous research [17]–[19], [22], [23]. However, the load often presents a certain degree of nonresistive feature with a reactive component besides the resistance, which can introduce a large error at high frequency operation if ignored. Mostly, the load in IPT system can be reasonably considered as a resistive load R_L in series with an equivalent series inductance (ESL) *L*. Therefore, an equivalent impedance Z_L is used in this research.

D. Two Modes of Operation

As shown in Fig. 1, a controllable ac switch *S* is formed by two semiconductor switches (e.g., IGBTs or MOSFETs). The compensation capacitor C_2 is added by controlling the ON and OFF states of the switch *S* to make the IPT system work at two operating modes with different compensation capacitors. These two circuit operating modes will be measured online and analyzed for system identification, as will be discussed in the following sections.

In designing the circuit parameters, the value of C_2 needs to make the frequency of the system and the loop current have an obvious change to be easily measurable. On the other hand, the value of C_2 should not be too large in order to avoid causing too much change of the power flow and too high stress on the circuit components.

III. Load Identification Model

A. Necessary Concepts and Assumptions

Before the theoretical analysis of the basic circuit topology of SS-type IPT system (Fig. 1) is conducted, the following concepts and assumptions need to be clarified:

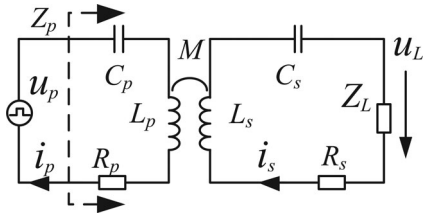

Fig. 2. The equivalent circuit model of SS IPT system.

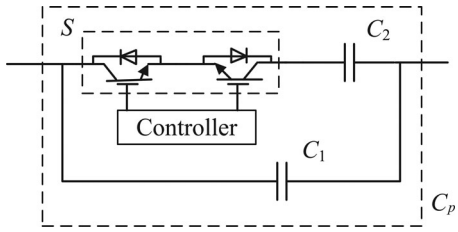

Fig. 3. The schematic of capacitance switching.

1) *The primary side resonance:* The primary side resonance means that the total reactance of the primary side impedance, including the reflected impedance of the secondary, is zero.
2) *Loss analysis:* There are mainly copper loss in the coils, the loss of the semiconductor switches and the core loss in an IPT system. When the system works in soft-switching mode, the switching loss can be ignored. Among all the above power losses, the copper loss in coils takes the major portion, so we just consider the copper loss in the system modeling.
3) *The parameters of the power pick-up circuit:* The pick-up circuit is composed of a secondary resonance network and load. This paper assumes that the power pickup winding L_s and compensation capacitor C_s, etc., are known and fixed parameters, as they do not change much under normal operating conditions.

B. Basic Theory of Reflected Impedance

The equivalent impedance of the energy pick-up winding Z_s is composed of a real part and an imaginary part, and its reflected impedance is denoted as Z_r in the primary winding. The equivalent circuit model of SS IPT system can be described in Fig. 2.

The Z_r and Z_s can be expressed as

$$Z_s = j\omega L_s + \frac{1}{j\omega C_s} + j\,\mathrm{Im}\,Z_L + \mathrm{Re}Z_L + R_s \tag{2}$$

$$Z_r = \omega^2 M^2 / Z_s = \mathrm{Re}Z_r + j\,\mathrm{Im}\,Z_r. \tag{3}$$

The Z_L can be expressed as

$$Z_L = R_L + j\omega L. \tag{4}$$

The real part and imaginary part of reflecting impedance can be calculated by

$$\mathrm{Re}Z_r = \frac{\omega^2 M^2 (R_s + \mathrm{Re}Z_L)}{(R_s + \mathrm{Re}Z_L)^2 + (1/\omega C_s - \omega L_s - \mathrm{Im}Z_L)^2} \tag{5}$$

$$\mathrm{Im}Z_r = \frac{\omega^2 M^2 (1/\omega C_s - \omega L_s - \mathrm{Im}Z_L)}{(R_s + \mathrm{Re}Z_L)^2 + (1/\omega C_s - \omega L_s - \mathrm{Im}Z_L)^2}. \tag{6}$$

The energy consumed by the real part of the reflecting impedance is the energy transferred from the primary winding to the secondary winding, the imaginary part of the reflecting impedance is used to store and release energy together with the primary winding resonance. Thus, generally it is necessary for the system to work at full resonance to achieve unity power factor and maximum power transfer. Under ideal no load condition, the operating frequency of the system is the natural resonant frequency of both the primary and the secondary side, satisfying the relationship

$$\frac{1}{\omega_{\mathrm{ref}}^2} = L_p C_p = L_s C_s. \tag{7}$$

Under the full primary resonance, the imaginary part of the primary side is zero, so we can get the relationship

$$\omega L_p - \frac{1}{\omega C_p} + \mathrm{Im}Z_r = 0. \tag{8}$$

C. System Parameter Identification Model

The total impedance Z_p of energy transmitter side in Fig. 2 can be described as

$$Z_p = R_p + \mathrm{Re}Z_r + j\omega L_p + \frac{1}{j\omega C_p} + j\mathrm{Im}Z_r. \tag{9}$$

When the load is connected to the system, the relationship between the input voltage U_p and the primary resonant circuit current I_p under ZCS condition can be expressed as

$$I_p = \frac{U_p}{\mathrm{Re}Z_r + R_p}. \tag{10}$$

The proposed method in this paper is for steady-state identification. The schematic of the capacitance switching part is enlarged and shown in Fig. 3. The change in the total compensation capacitance C_p by switching *S* makes the system work in two different operation modes.

In the design of the system parameters, the whole system is designed to be in full resonance when *S* if OFF and only the capacitor C_1 is in place. C_2 is added into the system when switch *S* is turned ON and the primary circuit is detuned. The inverter operating frequency is adjusted by detecting the current zero crossings to make the system work under the primary resonant state. If the harmonics are ignored, the square voltage of inverter and loop current are in phase and the current waveform is in approximate sine wave, therefore both of them can be calculated by using RMS values. The system works under two different sets of parameters because of the changing of compensation capacitor in the primary loop. Combined with the equation of impedance and system operating parameters, we can establish the equations with mutual inductance and load, and ultimately achieve the mutual inductance and load identification. When the capacitors C_1 and C_2 are both in the system, the natural

resonance frequency of the primary side becomes ω_{ref1}, satisfy the following relationship:

$$\frac{1}{\omega_{\mathrm{ref1}}^2} = L_p \cdot (C_1 + C_2). \tag{11}$$

Operating Model 1: The primary side is only compensated by C_1 when the switch *S* is turned OFF, the resonance frequency of primary side is ω_1, and then the system reflected impedance is

$$Z_{r1} = \omega_1^2 M^2 / Z_s. \tag{12}$$

The first RMS I_{p1} of the energy transmitter can be described as

$$I_{p1} = \frac{U_p}{\mathrm{Re}Z_{r1} + R_p}. \tag{13}$$

Operating Model 2: The capacitor C_2 is incorporated in circuit when the switch *S* is turned on. The frequency is adjusted by the controller to make the primary part of the system resonate, and then the reflected impedance can be written as

$$Z_{r2} = \omega_2^2 M^2 / Z_s. \tag{14}$$

The second RMS I_{p2} of the energy transmitter can be described as

$$I_{p2} = \frac{U_p}{\mathrm{Re}Z_{r2} + R_p}. \tag{15}$$

When the system operates under ZCS condition, the imaginary part of primary circuit is zero

$$\mathrm{Im}Z_{r1} + \omega_1 L_p - 1/\omega_1 C_1 = 0 \tag{16}$$

$$\mathrm{Im}Z_{r2} + \omega_2 L_p - \frac{1}{\omega_2 (C_1 + C_2)} = 0. \tag{17}$$

The following results can be obtained by integrating the above formulas

$$L = \frac{\alpha \cdot \beta + \gamma \cdot \lambda}{\omega_1 \cdot \alpha - \omega_2 \cdot \gamma} \tag{18}$$

$\alpha, \beta, \gamma, \lambda$ in (18) are given as follows:

$$\alpha = \mathrm{Im}Z_{r1} \cdot (0.9E_{\mathrm{DC}} - I_{p2}R_p) \cdot I_{p1} \tag{19}$$

$$\beta = \omega_2 L_s - \frac{1}{\omega_2 C_s} \tag{20}$$

$$\gamma = \mathrm{Im}Z_{r2} \cdot (0.9E_{\mathrm{DC}} - I_{p1}R_p) \cdot I_{p2} \tag{21}$$

$$\lambda = \omega_1 L_s - \frac{1}{\omega_1 C_s} \tag{22}$$

$$R_L = \frac{(0.9E_{\mathrm{DC}} - I_{p2}R_p) \cdot \left(\frac{1}{\omega_2 C_s} - \omega_2 L_s - \omega_2 L\right)}{\mathrm{Im}Z_{r2} \cdot I_{p2}} - R_s \tag{23}$$

$$M = \sqrt{\frac{\mathrm{Im}Z_{r2} \cdot \left[\mathrm{Re}Z_s^2 + \left(\frac{1}{\omega_2 C_s} - \omega_2 L_s - \omega_2 L\right)^2\right]}{\omega_2^2 \left(\frac{1}{\omega_2 C_s} - \omega_2 L_s - \omega_2 L\right)}}. \tag{24}$$

The $C_1, C_2, L_p, R_p, C_s, L_s, R_s$ in the formula (18)–(24) are the known parameters, the E_{DC}, I_{p1}, I_{p2}, ω_1, ω_2 can be measured when the system is in operation. The impedance equations of the loop current and the system operating frequency are established by switching the primary side compensating capacitor.

TABLE I
PARAMETERS OF IPT LOAD IDENTIFICATION SYSTEM

Parameters	Values
Primary compensation capacitance C_1	27.7 nF
Primary compensation capacitance C_2	4.8 nF
Primary resonant inductance L_p	362 uH
Inherent resistance of Primary circuit R_p	1.3 Ω
Secondary compensation capacitance C_s	65.9 nF
Secondary resonant inductance L_s	155 uH
Inherent resistance of Secondary circuit R_s	0.32 Ω
Input DC voltage E_{DC}	10 V

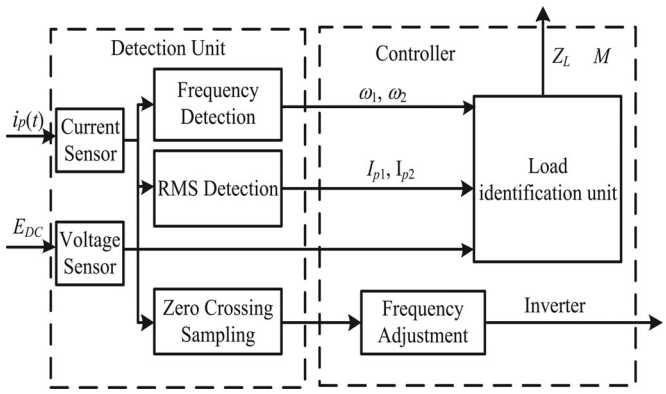

Fig. 4. The structure of the proposed identification method.

IV. SIMULATION AND EXPERIMENT STUDY

A. Parameters and Control Strategy

In order to verify the accuracy of the identification model of the IPT system, a SS-type IPT simulation model based on MATLAB is set up with reference to Fig. 1, the main parameters of the system are shown in Table I.

The control structure diagram illustrating the proposed identification method is shown in Fig. 4. The detection units include the resonant frequency detection, resonant current RMS sampling, resonant current zero crossing sampling, and the dc voltage measurement. The load identification controller includes load identification unit and frequency adjustment unit. The impedance equation of the load identification unit is established by using the RMS of primary loop current and the corresponding operating frequencies. The frequency adjustment unit is based on the zero crossing detection.

B. Simulation Results

The input dc voltage E_{DC} is applied to the system. Then the operating parameters of the system with C_1 only and both C_1 and C_2 are detected. We did a comparative analysis of the results obtained from simulation and practical experiment with real loads. The value of the ESL *L* in the simulation model is

TABLE II
PARAMETER IDENTIFICATION SIMULATION RESULTS WHEN THE LOAD R_L CHANGES FROM 10 TO 50 Ω

Load R_L	ESL L	Identified M	Identified R_L	Identified L
10 Ω	3.50 uH	35.20 uH	10.12 Ω	3.43 uH
20 Ω	4.86 uH	35.18 uH	20.14 Ω	4.78 uH
30 Ω	6.81 uH	35.16 uH	30.04 Ω	6.73 uH
40 Ω	8.94 uH	35.13 uH	39.96 Ω	8.85 uH
50 Ω	11.40 uH	35.11 uH	49.97 Ω	11.31 uH

TABLE III
PARAMETER IDENTIFICATION SIMULATION RESULTS WHEN THE M CHANGES FROM 30 TO 50 UH

Mutual Inductance M	Identified M	Identified R_L	Identified L
30 uH	30.11 uH	30.01 Ω	6.76 uH
35 uH	35.16 uH	30.04 Ω	6.73 uH
40 uH	40.24 uH	30.09 Ω	6.72 uH
45 uH	45.33 uH	30.13 Ω	6.70 uH
50 uH	50.45 uH	30.19 Ω	6.69 uH

taken from accurate measurement of an actual wound power resister for high frequency operation. So the identification results obtained in this research include the parameter R_L, the mutual parameter *M,* and the ESL *L* in the actual load. Table II shows the system parameter identification simulation results when *L* is taken into consideration, the targeted mutual inductance is 35 uH and the load variation range from 10 to 50 Ω. The results show that the largest identification error of R_L is 1.2%; the maximum identification error of *M* is 0.6%, the maximum identification error of *L* is 2.0%.

The simulation results for variable mutual inductance are shown in Table III. The targeted load is 30 Ω and its ESL *L* is 6.81 uH, and the mutual inductance changes from 30 to 50 uH. The maximum identification error of *M* is 0.9%; the maximum identification error of R_L is 0.6%; the maximum identification error of *L* is 1.7%.

C. Comparison of Identification Results With and Without Considering the ESL

If we ignore the ESL of the load *L* mentioned in Section II, we can get simplified equations from formula (23) and (24)

$$R_L = \frac{(0.9E_{\mathrm{DC}} - I_{p2}R_p)\left(\frac{1}{\omega_2 C_s} - \omega_2 L_s\right)}{\mathrm{Im}Z_{r2}\cdot I_{p2}} \tag{25}$$

$$M = \sqrt{\frac{\mathrm{Im}Z_{r2}\left[ReZ_s^2 + \left(\frac{1}{\omega_2 C_s} - \omega_2 L_s\right)^2\right]}{\omega_2^2\left(\frac{1}{\omega_2 C_s} - \omega_2 L_s\right)}}. \tag{26}$$

The relationship of the two operating models is not needed in formulas (25), (26). The operating parameters after the switching are directly used to calculate the load resistance. We made a comparison between taking consideration of ESL *L* and ignoring it. Since the energy is consumed by the resistive components in the actual circuit, we are more concerned about the load resistance R_L and mutual inductance *M*. The simulation parameters are the same with the simulation model with *L*. The results are shown in Fig. 5.

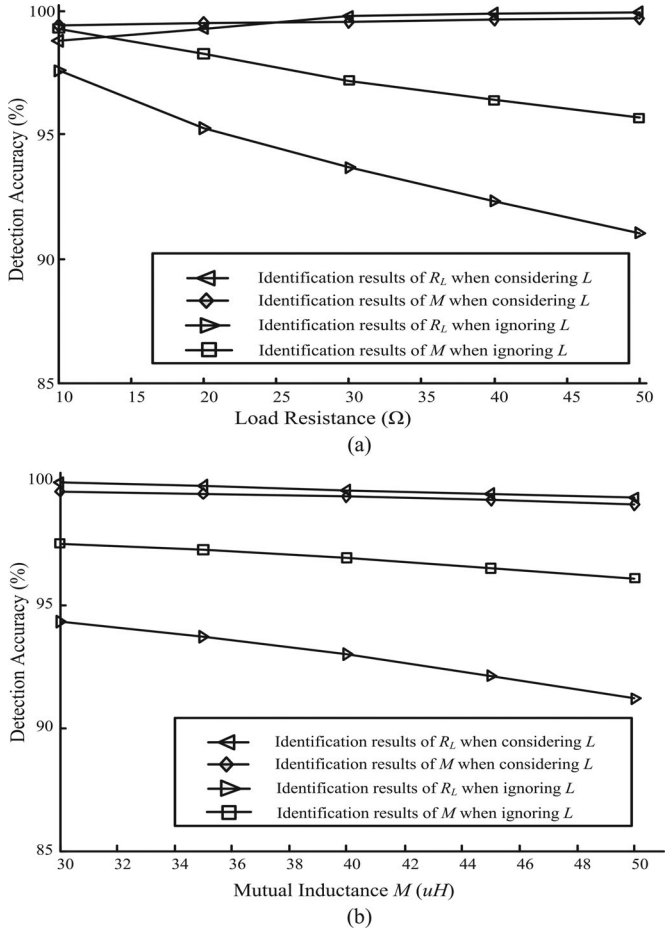

Fig. 5. The comparison results of considering *L* and ignoring *L*. (a) Different equivalent load resistance R_L. (b) Different mutual inductance *M*.

As shown in Fig. 5, the load identification accuracy of considering the series inductance *L* is higher than that not considering the *L*. When coupling the operating parameters before and after the capacitor switching and considering that there is a slightly nonresistance ingredient in the actual system, it can reduce the error between ideal formula calculation and actual circuit operating parameters, make the results more accurate. Because the frequency and current in the primary side will be affected by the resistance R_L and *L* at the same time, considering the existence of the reactive component of the load can make the analysis and calculation of the circuit closer to the actual situation, thereby getting more accurate results. It should be noted that in practical operation both of the load and mutual inductance can change at the same time, although for easy presentation Fig. 5 shows the situations when only one of them is varied each time.

D. Experimental Results

A load identification experimental platform based on the topology shown in Fig. 1 is built and practical tested in this

TABLE IV
PARAMETER IDENTIFICATION EXPERIMENT RESULTS WHEN THE LOAD R_L CHANGES FROM 10 TO 50 Ω

Load R_L	ESL L	Identified M	Identified R_L	Identified L
10 Ω	3.50 uH	37.50 uH	10.48 Ω	3.35 uH
20 Ω	4.86 uH	36.60 uH	19.59 Ω	4.67 uH
30 Ω	6.81 uH	36.02 uH	29.28 Ω	6.62 uH
40 Ω	8.94 uH	34.21 uH	38.63 Ω	8.71 uH
50 Ω	11.40 uH	33.57 uH	48.20 Ω	11.12 uH

TABLE V
PARAMETER IDENTIFICATION EXPERIMENT RESULTS WHEN THE M CHANGES FROM 30 TO 50 UH

Mutual inductance M	Identified M	Identified R_L	Identified L
30 uH	29.22 uH	29.64 Ω	6.59 uH
35 uH	36.02 uH	29.28 Ω	6.62 uH
40 uH	40.56 uH	29.47 Ω	6.66 uH
45 uH	45.96 uH	30.37 Ω	6.93 uH
50 uH	50.76 uH	30.45 Ω	6.97 uH

paper, the FPGA chip (Altera Cyclone II EP2C5T144C8) was selected as a controller of the load identification system. A comparator LM311 and phase correction circuit was used to achieve ZCS and an analog to digital converter chip ADS7841 was used to sample the current and voltage of the energy transmitter. Table IV shows the identification results when the mutual inductance is 35 uH and the load change varies 10 to 50 Ω. And it is found that the maximum identification error of M is 7.1%; the maximum identification error of R_L is 4.8%; the maximum identification error of L is 4.3%.

Table V shows the experiment of results when the load is 30 Ω and its ESL L is 6.81 uH, the mutual inductance changes from 30 to 50 uH. The maximum identification error of M is 2.9%; the maximum identification error of R_L is 2.4%; the maximum identification error of L is 3.2%.

These experimental results verified the feasibility and accuracy of the proposed load detection method with mutual inductance variations. As there are always some measurement errors in the actual system and we ignored the losses of the semiconductor switching devices, the experimental results of the load and mutual inductance are slightly lower than the simulation results which are further lower than the ideal theoretical results. To further improve the accuracy, a more accurate system model can be built with improved filtering algorithms to reduce the measurement errors.

In addition, it should be noted that the proposed method in this paper is suitable for steady-state identification of the system with relatively fixed parameters. Apart from R_L and M, other circuit parameter variations of an IPT system are very small under normal circuit operating conditions so their effect is very small. The additional switching capacitor is required only when the system needs to identify the load and mutual inductance. When the load identification is completed, the additional capacitor circuit will be turned OFF, so the circuit will go back to its original state. Normally it takes about 50 ms to complete an identification cycle. From power transfer point of view, if the magnetic coupling and power demand of the load changes too frequently, the frequent switching needed for the load identification may affect the continuous and stable operation of the original IPT system.

V. CONCLUSION

This paper presents a steady-state load identification method to identify the load and mutual inductance of an IPT system. The system works on two modes of operation by switching an additional compensating capacitor in the primary side of the circuit. The controller adjusts the frequency of the system to achieve primary side resonance. The identification results can be obtained according the operating parameter relationships between the two modes. An equivalent inductance L is considered in the process of establishing the model because of the load works at the condition of high frequency. It is proved that the accuracy of the identification results which considered L have an improvement. A simulation model and experimental platform are developed based on the theoretical analysis of the proposed method. The simulation and experimental results demonstrate that the method can effectively identify the load and mutual inductance parameters with good accuracy. Apart from the example SS-type IPT system, the method can also be extended to other types of IPT systems.

REFERENCES

[1] S. Raju, R. Wu, M. Chan, and C. P. Yue, "Modeling of mutual coupling between planar inductors in wireless power applications," *IEEE Trans. Power Electron.*, vol. 29, no. 1, pp. 473–480, Jan. 2014.
[2] H. H. Wu, G. A. Covic, J. T. Boys, and D. J. Robertson, "A series-tuned inductive-power-transfer pickup with a controllable AC-voltage output," *IEEE Trans. Power Electron.*, vol. 26, no. 1, pp. 98–109, Jan. 2011.
[3] M. Pinuela, D. D. Yates, S. Lucyszyn, and P. D. Mitcheson, "Maximizing dc-to-load efficiency for inductive power transfer," *IEEE Trans. Power Electron.*, vol. 28, no. 5, pp. 2437–2447, May 2013.
[4] S. Li and C. C. Mi, "Wireless power transfer for electric vehicle applications," *IEEE J. Emerg. Sel. Topics Power Electron.*, vol. 3, no. 1, pp. 4–17, Mar. 2015.
[5] J. Shin, S. Shin, Y. Kim, S. Ahn, S. Lee, G. Jung, S. J. Jeon, and D. H. Cho, "Design and implementation of shaped magnetic-resonance-based wireless power transfer system for roadway-powered moving electric vehicles," *IEEE Trans. Ind. Electron.*, vol. 61, no. 3, pp. 1179–1192, Mar. 2014.
[6] M. Budhia, J. T. Boys, G. A. Covic, and C. Y. Huang, "Development of a single-sided flux magnetic coupler for electric vehicle IPT charging systems," *IEEE Trans. Ind. Electron.*, vol. 60, no. 1, pp. 318–328, Jan. 2013.
[7] J. Huh, S. W. Lee, W. Y. Lee, G. H. Cho, and C. T. Rim, "Narrow-width inductive power transfer system for online electrical vehicles," *IEEE Trans. Power Electron.*, vol. 26, no. 12, pp. 3666–3679, Dec. 2011.
[8] K. M. Silay, C. Dehollain, and M. Declercq, "Inductive power link for a wireless cortical implant with biocompatible packaging," in *Proc. IEEE Sens. Conf.*, Kona, HI, USA, Nov. 2010, pp. 94–98.
[9] R. Wu, S. Raju, M. Chan, J. K. O. Sin, and C. P. Yue, "Silicon-embedded receiving coil for high-efficiency wireless power transfer to implantable biomedical ICs," *IEEE Electron Device Lett.*, vol. 34, no. 1, pp. 9–11, Jan. 2013.
[10] S. Ping, A. P. Hu, S. Malpas, and D. Budgett, "A frequency control method for regulating wireless power to implantable devices," *IEEE Trans. Biomed. Circuits Syst.*, vol. 2, no. 1, pp. 22–29, Mar. 2008.
[11] P. J. Chen, S. Saati, R. Varma, M. S. Humayun, and Y. C. Tai, "Wireless intraocular pressure sensing using micro fabricated minimally invasive flexible-coiled LC sensor implant," *J. Microelectromech. Syst.*, vol. 19, no. 4, pp. 721–734, Aug. 2010.

[12] E. Waffenschmidt, "Wireless power for mobile devices," in *Proc. IEEE Int. Telecommun. Energy Conf.*, Amsterdam, Netherlands, Oct. 2011, pp. 1–9.
[13] S. Li, W. Li, J. Deng, T. D. Nguyen, and C. C. Mi, " A double-sided LCC compensation network and its tuning method for wireless power transfer," *IEEE Trans. Veh. Technol.*, DOI 10.1109/TVT.2014.2347006, to be published.
[14] C. Y. Huang, J. T. Boys, G. A. Covic, and M. Budhia, "Practical considerations for designing IPT system for EV battery charging," in *Proc. IEEE Vehicle Power Propulsion Conf.*, 2009, pp. 402–407.
[15] C. S. Tang, Y. Sun, X. Dai, Y. G. Su, and Z. H. Wang, "Extended stroboscopic mapping (ESM) method: A soft-switching operating points determining approach of resonant inverters," in *Proc. IEEE Int. Conf. Sustainable Energy Technol.*, 2010, pp. 1–5.
[16] A. P. Sample, D. A. Meyer, and J. R. Smith, "Analysis, experimental results, and range adaptation of magnetically coupled resonators for wireless power transfer," *IEEE Trans. Ind. Electron.*, vol. 58, no. 2, pp. 544–554, Feb. 2011.
[17] X. Dai, Y. Sun, C. S. Tang, Z. H. Wang, Y. G. Su, and Y. L. Li, "Dynamic parameters identification method for inductively coupled power transfer system," in *Proc. IEEE Int. Conf. Sustainable Energy Technol.*, 2010, pp. 1–5.
[18] Z. H. Wang, Y. P. Li, Y. Sun, C. S. Tang, and X. Lv, "Load detection model of voltage-fed inductive power transfer system," *IEEE Trans. Power Electron.*, vol. 28, no. 11, pp. 5233–5243, Nov. 2013.
[19] Z. H. Wang, X. Lv, Y. Sun, X. Dai, and Y. P. Li, "A simple approach for load identification in current-fed inductive power transfer system," in *Proc. IEEE Int. Conf. Power Syst. Technol.*, 2012, pp. 1–5.
[20] A. Khaligh and S. Dusmez, "Comprehensive topological analysis of conductive and inductive charging solutions for plug-in electric vehicles," *IEEE Trans. Veh. Technol.*, vol. 61, no. 11, pp. 3475–3489, Aug. 2012.
[21] J. L. Villa, J. Sallan, J. F. Sanz Osorio, and A. Llombart, "High-misalignment tolerant compensation topology for ICPT systems," *IEEE Trans. Ind. Electron.*, vol. 59, no. 2, pp. 945–951, Feb. 2012.
[22] C. Hua, L. M. Shi, and Y. H. Li, "Harmonic-based phase-shifted control of inductively coupled power transfer," *IEEE Trans. Power Electron.*, vol. 29, no. 2, pp. 594–602, Feb. 2014.
[23] S. Y. R. Hui, W. Zhong, and C. K. Lee, "A critical review of recent progress in mid-range wireless power transfer," *IEEE Trans. Power Electron.*, vol. 29, no. 9, pp. 4512–4520, Sep. 2014.

Yu-Gang Su (M'09) received the B.E. and M.E. degrees in industry automation, and the Ph.D. degree in control theory and control engineering from Chongqing University, Chongqing, China, in 1985, 1993, and 2004, respectively.

From 2008 to 2009, he was a Visiting Scholar at the University of Queensland, Brisbane, Australia. He is currently a Professor at the College of Automation, Chongqing University. His research interests include power electronics, control theory and applications, wireless power transfer.

Hong-Yang Zhang received the B.E. degree in automation from Chongqing University, Chongqing, China, in 2012, where he is currently working toward the M.E. degree in control science and engineering.

He joined the Power Electronics and Control Laboratory in Chongqing University, as a Student, in 2012. His research interests include automatic control and practical engineering applications in wireless power transfer.

Zhi-Hui Wang (M'09) received the B.E. and M.E. degrees in automation, and the Ph.D. degree in control theory and control engineering from Chongqing University, Chongqing, China, in 2003, 2006, and 2009 respectively.

He is currently an Associate Professor at the College of Automation, Chongqing University. His research interests include fundamental investigations and practical engineering applications in efficient high-power converters and wireless power transfer.

Aiguo Patrick Hu (M'01–SM'07) received the B.E. and M.E. degrees in electrical engineering from Xian JiaoTong University, China, in 1985 and 1988, respectively and the Ph.D. degree in Electrical and Electronic Engineering from the University of Auckland, Auckland, New Zealand, in 2001 after migrating to New Zealand in 1996.

He is currently an Associate Professor at the Department of Electrical and Electronic Engineering, University of Auckland, and also a Guest Professor at Chongqing University, Chongqing, China. He holds 15 patents in wireless power transfer and microcomputer control technology, published more than 130 referred journal and conference papers, authored the first monograph on wireless inductive power transfer technology. His research interests include wireless power transfer and application of power electronics in renewable energy systems.

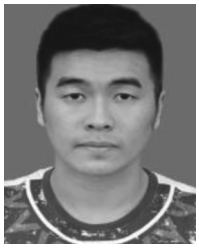

Long Chen received the B.E. degree in medical information from Southern Medical University, Guangzhou, China, in 2011. He is currently working toward the Ph.D. degree in control theory and control engineering from the College of Automation, Chongqing University, Chongqing, China.

His research interests include the load identification and optimization of wireless power transfer system.

Yue Sun (M'07) received the B.E. degree in electrical engineering, the M.E. degree in industry automation, and the Ph.D. degree in mechanical electrical integrated manufacturing from Chongqing University, Chongqing, China, in 1982, 1988, and 1995, respectively.

In 1997, he has been a Senior Visiting Scholar in France for one year. He is currently a Professor at the State Key Laboratory of Power Transmission Equipment & System Security and New Technology, and the College of Automation, Chongqing University, Chongqing, China. His research interests include automatic control, wireless power transfer and power electronics applications.